THE JOURNAL OF PHYSICAL CHEMISTRY C

Article

pubs.acs.org/JPCC

Strong Field Ionization of β-Estradiol in the IR: Strategies To Optimize Molecular Postionization in Secondary Neutral Mass Spectrometry

Andrew Kucher,[†] Andreas Wucher,[‡] and Nicholas Winograd*[,†]

[†]Chemistry Department, The Pennsylvania State University, 104 Chemistry Building, University Park, Pennsylvania 16802, United States

[‡]Fakultaet fuer Physik, Universitaet Duisburg-Essen, 47048 Duisburg, Germany

Supporting Information

ABSTRACT: Strong field laser photoionization of β-estradiol in the 10^{13}–10^{15} W/cm^2 intensity range at wavelengths between 1200 and 2000 nm was examined for both evaporated gas phase molecules and neutral species sputtered from a solid surface under bombardment with 20 keV C_{60}^+ ions. It is shown that the ionization efficiency is saturated at laser intensities of the order of 10^{13} W/cm^2, while laser-induced photofragmentation is found to strongly increase between 10^{13} and 10^{14} W/cm^2 and stay constant at higher intensities. These findings suggest a strategy to improve the postionization efficiency by defocusing the laser beam in order to sample a larger fraction of the sputtered plume, while at the same time optimizing the conditions for intact photoionization of the sputtered molecules. The results reveal a substantial enhancement of the signal of intact postionized molecular ions to a level an order of magnitude above that of the corresponding secondary ions. They also provide an experimental estimate of $\sim 2.5 \times 10^{-2}$ as an upper bound for the ion fraction (secondary ion formation probability) of the sputtered molecules.

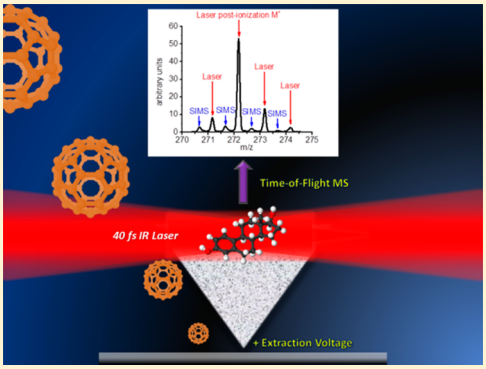

INTRODUCTION

Secondary ion mass spectrometry (SIMS) is a sensitive surface analysis technique which involves the probing of surfaces by an evolving selection of ion beams[1,2] and the analysis of the ejected ions with a high-resolution mass spectrometer.[3] The development of cluster primary ion sources has greatly extended the utility of SIMS for biological applications.[4] However, low secondary ion yields of sputtered molecules (estimated to be in the range of 10^{-3}–10^{-7} for organics), and their susceptibilities to matrix effects, have persisted since the inception of SIMS.[5] For biological studies, low concentrations of analytes present in the submicron analysis regime also provide measurement challenges. To address these problems, laser postionization (LPI) of the flux of undetectable sputtered neutral molecules has been a developing complement to the SIMS experiment for several decades.[6−12]

Heretofore secondary neutral mass spectrometry (SNMS) has had its greatest and most general success in elemental analysis,[13,14] while biologically relevant organic molecules remain problematic. To date, several LPI schemes have been implemented, involving single (SPI)[15,16] and multiple photon (MPI)[17−21] absorption methods, which have found notable success in some applications. However, limitations inherent to their ionization mechanisms have limited their generality. In SPI, successful photoionization of a molecule without significant fragmentation is largely determined by Franck–Condon factors and is only efficient if the molecule does not significantly change its geometric configuration upon ionization. In addition, typical molecular ionization potentials (8–12 eV) generally require photon energies associated with VUV radiation which is not readily commercially available. In MPI, on the other hand, excess photon absorption beyond that required for ionization generally leads to extensive dissociation.

The search for a universal LPI source is ongoing and has recently advanced into a fundamentally different regime. Instead of tailoring photons for absorptive ionization, this novel approach utilizes the electric fields induced by powerful ultrashort laser pulses to exceed Coulomb fields in molecules. This switch is necessary since previous attempts at LPI using shorter wavelengths[19−21] or longer pulses[8] only yield molecular ions when the laser power is reduced to near threshold, and the ionization efficiency is impractically low. The processes occurring during strong field ionization (SFI) are an area of ongoing spectroscopic and theoretical research, as they underpin the emerging field of attosecond electron dynamics.[22,23] Current understanding of SFI is based on the interplay of two distinct ionization regimes, described as adiabatic and nonadiabatic dynamics.[22,24−37] Molecular and laser properties

Received: August 9, 2014
Revised: September 24, 2014
Published: October 7, 2014

   dx.doi.org/10.1021/jp5080708 | J. Phys. Chem. C 2014, 118, 25534–25544

affect the transition between them and the final outcome of each, be it intact ionization or heavy fragmentation.

Described as involving tunneling or barrier suppression, adiabatic ionization is generally treated as a quasi-static field phenomenon involving a single active electron, which—at least to first order—should be independent of wavelength.[38] It is often believed not to couple energy from the laser field into electronic excitation of the molecule,[24] but it has been shown that this picture is not always accurate. Field ionization may occur from the highest occupied molecular orbital (HOMO), leaving a ground state cation, or from inner states (HOMO−1, etc.), leaving behind an excited state cation. If the excitation energy is above the dissociation threshold of the molecule, fast internal conversion may then lead to fragmentation. Molecular bonding plays a defining role in the extent of excited state cation formation and hence also the resulting fragmentation during adiabatic ionization.[22]

Despite not being universally free of fragmentation, the adiabatic regime is preferred for LPI, since more intact ions are created than when employing nonadiabatic multielectron excitation (NME), the competing ionization mechanism in SFI. During NME, the rate of change of the laser field becomes too large for the molecule to adjust to the momentary field in a quasi-static manner, leading to a collective response of the entire electron cloud which may be accompanied by substantial electronic excitation. An important parameter in this context is the (dynamic) polarizability of the molecule, which depends upon molecular properties like size and electronic structure as well as the laser wavelength and intensity. As a general trend, one finds that NME becomes increasingly pronounced for molecules of increasing size, when irradiated by shorter wavelengths and higher intensities.[26,28] Hence, there is a preference to focus on using IR wavelengths rather than wavelengths in the visible region of the spectrum.

Ionization and fragmentation in the NME regime are generally described as a two-step process.[27,28] First, the strong laser field dynamically Stark shifts and broadens molecular states, with all excited states mixing into a quasi-continuum (QC). A ground state electron promoted into the QC rapidly absorbs energy from the laser field in a plasma-like fashion until it escapes over the barrier.[25,26] Once ionized, the NME process can be repeated again in the molecular cation, leading to the population of high-lying excited states, many of which are repulsive and lead to fragmentation. As a consequence, the relative role of NME is closely tied to the intensity and wavelength of the ionizing laser. For a number of gas phase molecules, the use of longer wavelengths, and tailored intensity ranges, have been shown to reduce NME and its associated photodissociation,[25,26] thereby producing quasi-adiabatic ionization and near fragment free mass spectra. In early applications of SFI to SNMS, similar behavior was observed for sputtered molecules, although the available intensity in those studies was limited to 10^{13} W/cm^2.[12]

The goal of the present work is to probe the SFI regime with a more expansive set of laser conditions than previously published for an organic molecule, with the aim of optimizing its use for molecular postionization in SNMS. In doing so, we chose β-estradiol (Scheme 1) as a model system for the sterol class of biologically important molecules. Using a laser system capable of producing tunable infrared radiation at wavelengths between 1160 and 2580 nm and peak power densities of up to 10^{15} W/cm^2, we examine the role of wavelength and laser intensity with respect to intact photoionization and photofragmentation. In doing so, we geometrically restrict the effective ionization volume for these studies to the Rayleigh range of the laser focus, thereby limiting the laser intensity variation to only the radial dimension. This produces a cylindrical focal geometry which has been well described by established analytical equations.[39]

Scheme 1. β-Estradiol m/z 272.4, with the Structure to the Left of the Dashed Line Representing the m/z 145 Fragment

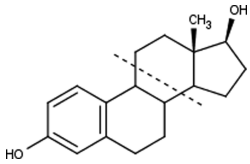

We began our investigation with gas phase molecules, since an important feature of the ion induced desorption process is that sputtered molecules may contain rather large amounts of internal energy, which may in principle alter their response to the laser pulse. In order to decouple the influence of preexisting vibrational or electronic excitation of the neutral precursor from laser-induced excitation and fragmentation processes, we compare the response of the sputtered molecules with that measured for evaporated gas phase molecules, utilizing the fact that the latter exhibit only a negligibly small thermal excitation. Using the measured molecule response, we then identify optimum conditions with respect to laser wavelength and intensity that ensure the largest possible postionization efficiency of the intact molecule along with minimal photofragmentation. We will show that it is in all cases favorable to use a relatively low laser intensity that is closely above a threshold value which can be directly determined from the measured data. As a consequence, it is possible to optimize the postionization efficiency by defocusing the laser beam such that the optimum intensity is established in the center of the beam. Using this strategy, we demonstrate that the employed laser system can increase the signal of molecular ions generated by postionization in SFI-SNMS to an order of magnitude above that of the corresponding molecular secondary ion detected in SIMS. Discussing the overlap between the effective ionization volume sampled by the laser and the detectable plume of sputtered particles, we then derive an estimate of the maximum possible molecular ion signal enhancement achievable in a β-Estradiol SFI postionization experiment.

EXPERIMENTAL SECTION

The commercially available laser system employed in these experiments is based on chirped pulse amplification (Coherent Legend Elite Duo) and produces pulses of 40 fs duration at 800 nm wavelength, with a repetition rate of 1 kHz and an average power of 10 W. The pulse width is checked by frequency-resolved optical gating (FROG, Swamp Optics Grenouille 8-20-USB).[40] The laser output is used to pump a commercially available optical parametric amplifier (OPA, Light Conversion TOPAS-C-HE), the output wavelength of which is tunable in the 1160−2580 nm range, with a combined signal and idler conversion efficiency between 30% and 40% of the pump power.

The OPA consists of three amplification stages, with the first and third possessing a large effect on the output wavelength, in addition to the power. Therefore, the experimental intensity is adjusted using the second stage, specifically by changing the delay between the pump and seed pulses. This method has

dx.doi.org/10.1021/jp5080708 | J. Phys. Chem. C 2014, 118, 25534−25544

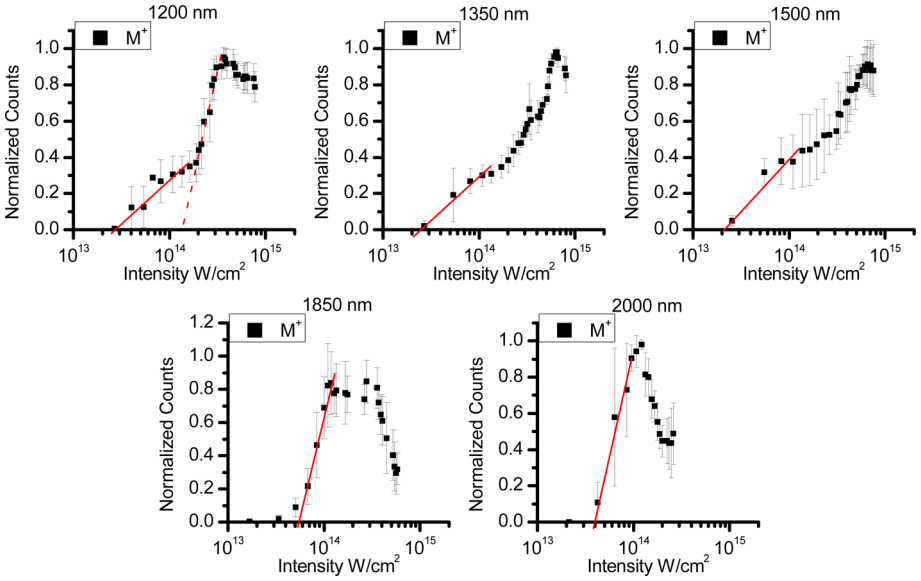

Figure 1. Gas phase ionization signal of β-estradiol molecular ion vs laser intensity in the 1200−2000 nm wavelength range. Superimposed lines: asymptotic straight line fits according to eq S1 in the Supporting Information.

almost no effect on the output wavelength and pulse width. The signal and idler outputs of the OPA are filtered with appropriate dichroic mirrors. The generated wavelengths are confirmed by detecting their (BBO crystal) frequency doubled light in an Ocean Optics USB 4000 spectrometer. They are focused into the mass spectrometer using a 150 mm (at 587.6 nm) focal length lens, which produces a 75 ± 25 μm focal diameter for all wavelengths. Ion collection is restricted to the Rayleigh range of the laser focus using a 600 μm wide slit placed perpendicular to the propagation direction of the laser beam and underneath the entrance to the time-of-flight spectrometer. As described in the Supporting Information, the well-known ionization behavior of high-purity xenon gas was used in order to calibrate the laser intensity.[41]

The TOF-SIMS instrument employed in these experiments has been described elsewhere.[42] Briefly, it consists of a 20 keV C_{60}^+ ion gun (Ionoptika IOG C60-20),[43] a reflectron mass spectrometer, a residual gas analyzer (Extor XT200M), a variable leak valve, and a temperature controllable sample stage. For the SNMS/SIMS experiments a 20 keV C_{60}^+ primary ion beam of 40−70 pA (dc current) was pulsed with a pulse width of 2000 ns for sputtering. The long primary ion pulse width was selected to optimize SNMS detection sensitivity across the examined mass range, as discussed previously.[44] The total ion dose applied during acquisition of the mass spectra was restricted to ~10^{12} ions/cm^2 in order to stay within the static limit. The instrument was operated in delayed extraction mode, with the sample at ground potential during ion bombardment and the ion extraction field being switched on immediately after the end of the primary ion pulse. During SNMS, positive secondary ions emitted from the surface were directed back toward the surface by a pulse of −2450 V and 150 ns duration applied to the sample stage prior to the introduction of the laser. The laser pulse was fired with a delay of about 60 ns after the start of the ion extraction pulse, in order to separate residual secondary ion signals from LPI generated peaks in the flight time spectrum. This is possible since the flight time zero for secondary ions is determined by the switching time of the extraction pulse, whereas for postionized neutrals it is determined by the laser pulse. During SIMS, the suppression pulse was omitted and secondary ions were extracted into the reflectron immediately after the conclusion of the primary ion pulse. In order to suppress the gas phase background signal generated by photoionization of species evaporated from the surface, the sample block was cooled to 100 K by passing liquid nitrogen through the holder stage. The operating pressure during SNMS was ~1×10^{-9} mbar.

Detector gain saturation[45] by ions below m/z 40 was encountered during SNMS experiments at laser intensities exceeding ~6×10^{13} W/cm^2. This is a critical phenomenon, since the detector requires a relatively long time to recover, thereby effectively precluding the detection of larger molecular species. To prevent saturation, a grid mounted above the MCP detector was pulsed to a potential exceeding the kinetic energy imparted to the photoions in the extraction field, with the pulse being timed such as to prevent the ions in the m/z 0−100 range from reaching the detector. As a result, since these ions never reach the detector, saturation effects are avoided.

High-purity β-estradiol (98% CAS 50-28-2) was purchased from Sigma-Aldrich. For SNMS experiments it was deposited onto Si shards and 400 mesh Ni London finder grids (Electron Microscopy Sciences) in a home-built vapor deposition chamber. During gas phase ionization experiments β-estradiol was pressed into indium foil, attached to the sample block, and heated to 343 K until a constant partial pressure (monitored by the residual gas analyzer trace of representative m/z 145 fragments) was established. The total instrumental pressure during these experiments never exceeded 3×10^{-8} mbar.

RESULTS AND DISCUSSION

The goal of the present work is to explore the role of laser intensity and wavelength for strong field photoionization of a sputtered organic molecule and utilize the results to optimize the postionization efficiency for generation of intact molecular ions in a laser-based SNMS experiment. To achieve this goal, it is important to carefully characterize the focal properties of the postionization laser along with the detection volume of the TOF instrument. As described in the Supporting Information, we use the SFI-signal measured for gas phase Xe atoms for that

dx.doi.org/10.1021/jp5080708 | J. Phys. Chem. C 2014, 118, 25534−25544

purpose, which can be compared with published experimental data in order to verify our experimental protocol and to calibrate the laser intensity. We then present measurements for gas phase β-estradiol produced by thermal evaporation at 343 K, which is treated as an approximation of the response of ground state molecules to the laser field. Subsequently, we investigate neutral molecules desorbed under C_{60}^+ ion bombardment, discussing the similarities and differences of their response in terms of the internal excitation generated during the sputtering process. Finally, we utilize the collective measurements to determine optimum postionization conditions and compare the resulting optimized SFI-SNMS molecular ion signal with that measured in SIMS in a model imaging experiment.

SFI of Gas Phase β-Estradiol. In contrast to atomic species, the response of molecules to a strong laser field is complicated by additional internal degrees of freedom. These modes can be excited in the course of the photoionization process, leading to neutral fragmentation or dissociative ionization if the excitation energy exceeds the dissociation threshold. In addition, the response can be strongly influenced by a pre-existing internal or electronic excitation of the neutral precursor, which might be substantial for sputtered molecules. In order to unravel both effects, it is therefore desirable to investigate the ionization behavior of gas phase molecules and compare it with that measured for the sputtered species. For that purpose, β-estradiol molecules were sublimed from the sample surface by heating the sample to 343 K, yielding a negligible average thermal excitation energy of ~0.03 eV as compared to the ionization potential.

The results are presented in Figure 1 and reveal mechanisms that are much more complex than those observed in atomic xenon (see Figure S1 in the Supporting Information), with seemingly two distinct ionization regimes separated by a transition region.

In the lower 10^{13}–10^{14} W/cm^2 range, the molecular ion signal increases with laser intensity at all wavelengths. As described in the Supporting Information, the quasi-linear rise observed in this regime indicates saturated ionization, and the concepts underlying eq S1 can be used in order to determine the saturation intensity I_{sat}. The resulting values, determined from the indicated straight lines, are listed in Table 1 and reveal a saturation intensity of the order of ~2×10^{13} W/cm^2 for 1200–1500 nm ionization. The calculated ionization potential of β-estradiol is 8.23 eV.[46] Using standard Ammosov–Delone–Krainov (ADK) theory,[38] a value of 2.5×10^{13} W/cm^2 is predicted for this ionization potential under adiabatic SFI conditions (see Figure 2), which agrees with the data in Table 1. It is, however, seen that the measured value slightly increases with increasing laser wavelength, a behavior which is not expected for a purely adiabatic ionization mechanism.

Table 1. Saturation Intensity I_{sat} Determined from the Straight Line Fits Indicated in Figures 1 and 5 for Strong Field Ionization of β-Estradiol at Different Laser Wavelengths[a]

	1200 nm	1350 nm	1500 nm	1850 nm	2000 nm
evaporated	2.5	2.2	2.1	4.0	3.6
sputtered	1.1	1.2	1.6	1.5	2.1

[a]Values are given in units of 10^{13} W/cm^2.

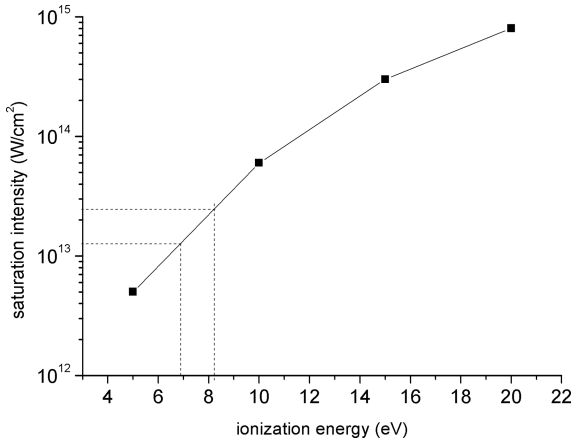

Figure 2. Saturation intensity for adiabatic SFI vs ionization potential predicted by ADK theory (data taken from ref 44).

Up to a laser intensity of 2×10^{14} W/cm^2 (as used in most studies published to date), the interpretation of the measured data would appear straightforward. Above that intensity, however, we find a complicated structure of the measured curves which clearly depends upon the wavelength. Probably the most prominent feature observed at the lowest wavelength of 1200 nm is an apparent onset of a second ionization mechanism. In principle, the formalism leading to the definition of I_{sat} as described in the Supporting Information could be used again, leading to a straight line with about twice the slope above the corresponding saturation intensity of ~2×10^{14} W/cm^2 (dotted line in Figure 1). A somewhat similar behavior is also observed at larger wavelengths up to 1500 nm, although the break is less pronounced. The onset of a second mechanism appears to be absent at longer wavelengths.

If the laser intensity approaches 10^{15} W/cm^2, all signals turn over and decrease with increasing laser intensity. An intuitive explanation of this phenomenon would be to assume that the molecular ion signal decays due to increasing fragmentation accompanying the ionization process. In order to examine this possibility, we present in Figure 3 the dependence of a prominent fragment signal at m/z 145. This fragment arises from bond scission of the molecule along the dashed line shown in Scheme 1. It is immediately evident that the fragments exhibit essentially the same behavior as the molecular ion and particularly show the same decrease at high intensity. Alternatively, it is possible that multiple ionization generates space charge within the ionization volume which is large enough to effectively modify the ion trajectories, thereby reducing the transmission of the spectrometer for all detected ions in the same way.

One might argue that m/z 145 is still a large fragment ion which may further decompose into smaller fragments in the course of the dissociation chain. To assess this possibility, the sums of all detected fragment signals with $m/z > 40$[a] for the example of two different wavelengths are plotted in the upper panels of Figure 4.

It is seen that the same laser intensity dependence is found for all fragments, thereby effectively ruling out laser-induced fragmentation as a cause of the observed signal decay. In fact, if we plot the ratio between molecular ion and the summed fragment signals in the lower panels of Figure 4, we find a decreasing trend at lower intensity which levels off above 10^{14} W/cm^2. In other words, the laser generated fragmentation

dx.doi.org/10.1021/jp5080708 | J. Phys. Chem. C 2014, 118, 25534–25544

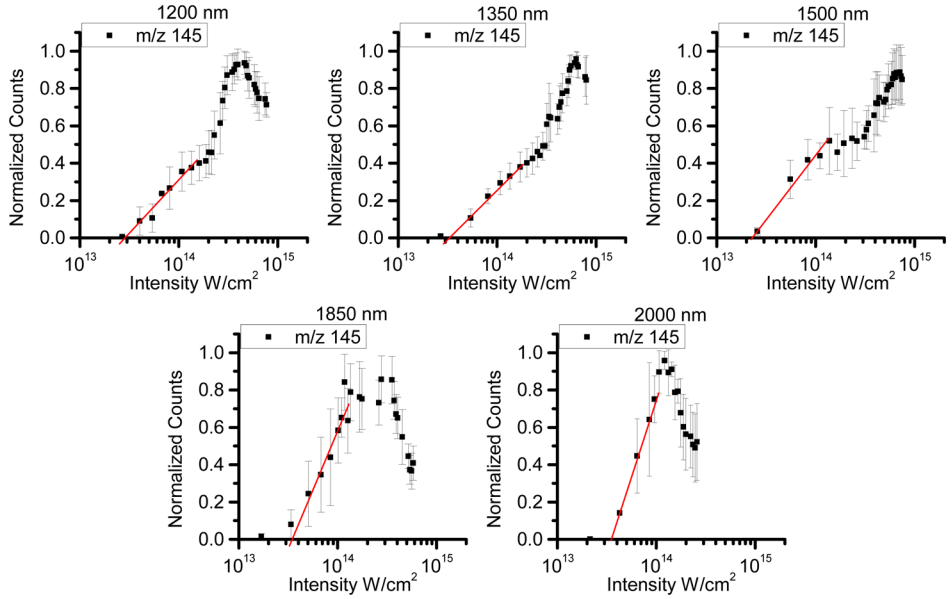

Figure 3. Gas phase ionization signal of β-estradiol m/z 145 fragment ions vs laser intensity in the 1200−2000 nm wavelength range. Superimposed lines: asymptotic straight line fits according to eq S1 in the Supporting Information.

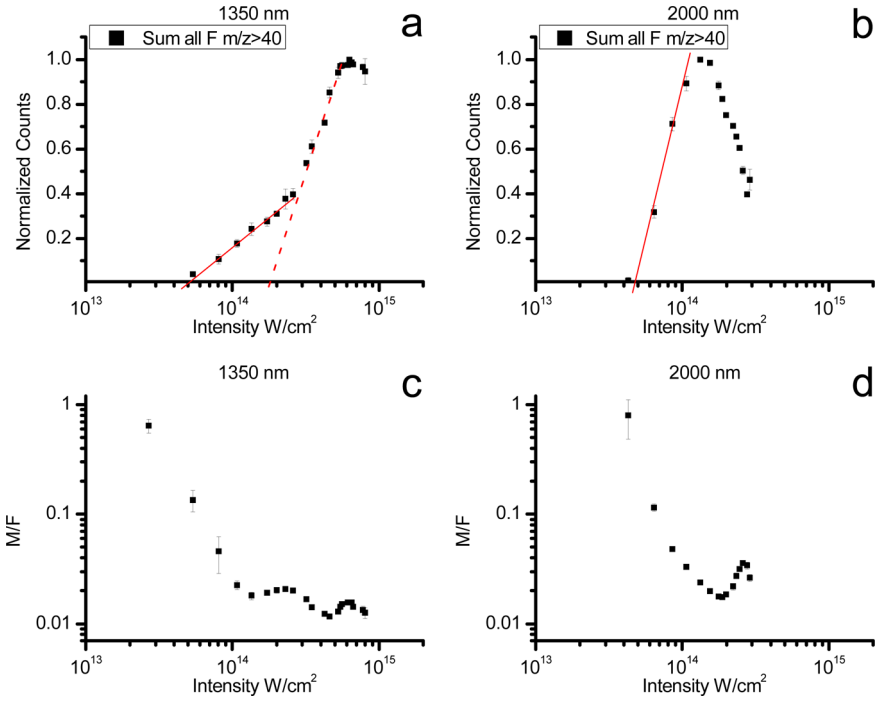

Figure 4. Gas phase ionization of β-estradiol. Upper panels: laser intensity dependence of the sum of all fragments larger than m/z 40 for (a) 1350 nm and (b) 2000 nm ionization. Superimposed lines: asymptotic straight line fits according to eq S1 in the Supporting Information. Lower panels: ratio of molecular ion to summed fragment ion signals ($>m/z$ 40) vs laser intensity for (c) 1350 nm and (d) 2000 nm ionization.

pattern appears to become almost constant in the limit of high intensity.

In this context, it should be pointed out that a similar deviation from the asymptotic straight line has been observed earlier,[39] where it was attributed to a Coulomb explosion-like fragmentation of multiply charged ions. Because of the kinetic energy release in such a process, the resulting fragments gain an orthogonal velocity component which may prevent them from being transmitted through the mass spectrometer, thereby reducing the detected fragment signal. In the low intensity regime of Figure 4, saturation values for the formation of m/z 145 fragments appear to be slightly above those for the molecular ion. This finding is even more pronounced for the sum of all fragments as indicated in Figure 4, which shows an apparent saturation intensity which is clearly higher than that of the molecular ion. In this context, it is important to note that—due to the short duration of the laser pulse—fragmentation can only occur via the production of an excited molecular ion which then fragments if the excitation energy imparted during the ionization process exceeds the dissociation threshold. Therefore, it is evident that dissociative ionization must be associated with a threshold energy that is larger than the ionization

dx.doi.org/10.1021/jp5080708 | J. Phys. Chem. C 2014, 118, 25534−25544

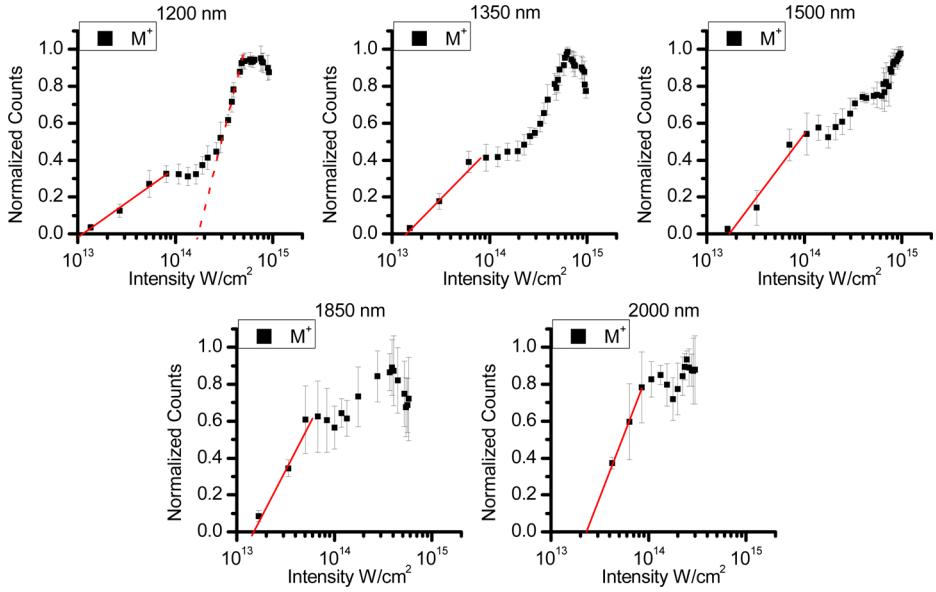

Figure 5. Postionization behavior of sputtered β-estradiol molecular ions in the 1200−2000 nm wavelength range. Superimposed lines: asymptotic straight line fits according to eq S1 in the Supporting Information.

potential of the intact molecule. Using the same reasoning as outlined above, one would intuitively expect the saturation intensity for dissociative ionization to be larger than that for the intact ionization of a molecule, which is in accordance with our experimental observation. Moreover, the fact that we observe linear behavior for the fragment sum indicates that the deviations from the expected linear dependence observed for the molecular ion and the m/z 145 fragment around 10^{14} W/cm^2 is caused by fragmentation.

SFI of Sputtered β-Estradiol. By contrasting gas phase ionization with analogous SNMS studies, it is possible to examine the effect that ion beam desorption has on the SFI mechanism in β-estradiol. This is essential for determining its practical utility, as sputtering can impart a degree of internal energy to the molecule which may alter the ionization mechanism and produce increased photodissociation. For example, an earlier LPI study of dopamine showed 4 eV of internal energy excitation induced by atomic Ga^+ sputtering, which drastically altered the photon order under multiphoton ionization of the molecule.[21] Similar observations have been made for sputtered metal clusters, which were shown to be ionized via single photon absorption at photon energies below the ground state ionization potential.[47−49]

The response of sputtered β-estradiol molecules desorbed by C_{60} ion bombardment is shown in Figure 5. At first glance, the observed laser intensity dependence looks very similar to that measured for evaporated molecules (Figure 1). There are, however, subtle differences that are noteworthy. First, we determine the saturation intensity as outlined above and find values that are consistently lower than those of the gas phase molecules (see Table 1). In line with the observations cited above, we attribute this finding to the internal excitation of the sputtered molecules, which may act to effectively lower their ionization potential.[49] As seen from Figure 2, standard ADK theory would relate the observed saturation intensity of about 1.3×10^{13} W/cm^2 to an ionization potential of ~7 eV, indicating an ionization active average internal energy of about 1.3 eV per molecule.[b] In light of similar data reported for sputtered metal clusters[47−49] as well as theoretical MD simulations of the molecule ejection process,[50] this value appears reasonable.

It is interesting to note that the onset of the second ionization mechanism appears to be nearly unchanged between evaporated and sputtered molecules (cf. dotted lines in Figures 1 and 5). As a consequence, the response curves of the sputtered molecules exhibit a plateau in the transition region which is much less pronounced for the gas phase molecules. At present, we can only speculate what may cause this break from the expected linear behavior. Since the asymptotic straight line simply reflects the ionization volume expansion, the deviation must be caused by a loss of molecular ion signal with increasing intensity in the center of the laser beam, probably by photofragmentation.

Another striking difference between the response curves measured for evaporated and sputtered β-estradiol is seen in the limit of large laser intensity. Particularly at longer wavelengths, the signal decay observed for evaporated molecules is much less pronounced for the sputtered species. This difference can be utilized to discuss the cause of the observed signal decay in more detail. In the ion desorption experiment, we observe significantly higher signals of low mass fragment ions than in the evaporation experiment. We attribute this to the fact that the sputtering process itself generates an abundant flux of neutral fragments. These fragments are subsequently ionized by the laser and contribute to the measured fragment ion spectrum. In fact, the sputtering experiment had to be performed under conditions where the low mass fragment signals were suppressed in order to avoid detector saturation (see Experimental Section). As a consequence, we conclude that any space charge created by laser generated photoions must be more severe in the sputtering experiment than in the gas phase experiment, thereby ruling out the space charge as a possible explanation for the observed signal decay. At present, it is unclear why the laser-induced fragmentation at intensities above 10^{15} W/cm^2 could be reduced for sputtered molecules. In order to gain further insight into the mechanisms that govern ionization and fragmentation in this high-intensity regime, it would be

dx.doi.org/10.1021/jp5080708 | J. Phys. Chem. C 2014, 118, 25534−25544

necessary to investigate correlations between the detection of different fragment ions and the liberated photoelectrons similar to the channel resolved above threshold ionization (CRATI) measurements published recently.[22] In addition, experiments using circularly polarized laser beams might help to differentiate between adiabatic and nonadiabatic ionization mechanisms. Such studies, however, are outside the scope of the present paper.

Optimizing SFI for SNMS of β-Estradiol. The fundamental studies reported above indicate that quasi-adiabatic ionization is observed for all examined wavelengths, as long as the intensity is restricted to 10^{13}–10^{14} W/cm^2. Moreover, the data show that the ionization efficiency saturates at ~10^{13} W/cm^2, making it in principle unnecessary to work at much higher laser intensity. At the same time, decreasing the intensity below ~10^{14} W/cm^2 leads to significant decrease of laser-induced fragmentation as shown in Figure 4. Moreover, a tightly focused laser beam needed to achieve high intensity intersects only a small part of the sputtered plume.

A strategy to optimize the useful molecular ion signal in SFI-SNMS is therefore to defocus the laser beam, decreasing its intensity and at the same time increasing the effectively sampled ionization volume. In principle, the data in Figure 4 suggest to reduce the laser intensity as much as possible in order to minimize photofragmentation. On the other hand, the laser intensity must remain sufficiently high to ensure efficient photoionization. In order to quantify the interplay between both contradicting requirements, we define the efficiency for intact photoionization by multiplying the measured molecular ion signal (M) with the survival probability against fragmentation (M/F) as displayed in the bottom panels of Figure 4. For a wavelength of 1350 nm as an example, the result is plotted in Figure 6, which shows that optimum conditions are obtained at a laser intensity of ~5 × 10^{13} W/cm^2.

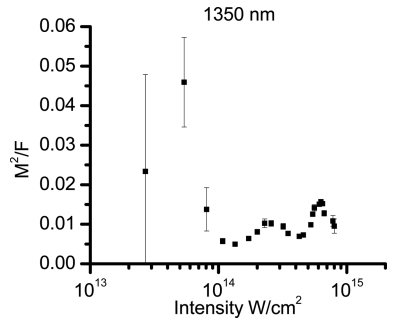

Figure 6. Efficiency for intact photoionization of β-estradiol vs laser intensity at 1350 nm calculated as described in the text.

In this context, it is necessary to estimate the overlap of a focused laser with the plume of material sputtered from the surface. Because of the emission angle and velocity distribution of the sputtered particles, the plume of neutral particles which can be ionized and detected by the mass spectrometer disperses with distance from the sample,[51] and due to sample stage design we are limited in how closely the laser beam can be brought to the surface. For the tightly focused laser, the lowest typically achievable height is ~500 μm, where the lateral diameter of a plume of sputtered material emerging form a point source at the bombarded surface is ~1000 μm. Obviously a 75 ± 25 μm laser focus, like the one employed in the above fundamental studies, will not overlap with a large portion of the sputtered flux. In addition, typical experiments often involve rastering the primary ion beam across the surface to image or to reduce the primary ion dose during data acquisition.

In a recent experiment to estimate the magnitude of the undersampling effect, we have scanned the focused laser beam in order to map the volume from which postionized neutral particles can be extracted and detected.[52] For sputtered In atoms emerging from an indium surface bombarded by the same C_{60}^+ ion beam as used here, we found that the tightly focused laser samples about 3% of the entire detectable sputtered plume.[52] The theory behind eq S1 in the Supporting Information shows that saturated ionization efficiency is reached at ~ eI_{sat}. At this intensity, the diameter of the effectively sampled ionization volume (i.e., the volume where the laser intensity $I \geq I_{sat}$) is equal to the beam diameter (i.e., $R' = R$), and the laser therefore samples a significantly larger portion of the sputtered plume.

In this context, one should note that even though the analysis is performed at relatively low laser intensity, it is still advantageous to employ a laser delivering the highest possible power in order to maximize the diameter of the defocused beam at a given intensity. In order to maximize the useful molecular ion signal of β-estradiol, we therefore use a wavelength of 1350 nm, since the highest intensity the OPA generates in our experiment (10^{15} W/cm^2) peaks at this wavelength. The saturation intensity determined here for β-estradiol molecules (~2 × 10^{13} W/cm^2) allows defocusing the laser beam to a spot diameter[c] of about ~322 μm (corresponding to R ~ 114 μm), now delivering a peak intensity of ~5 × 10^{13} W/cm^2. Note that this value is about equal to eI_{sat} as well as the value needed for optimum intact ionization efficiency as determined from Figure 6. Since the saturation intensity of β-estradiol is about the same as that measured for sputtered In atoms, we can use the indium data[52] to estimate that ~25% of the sputtered plume is sampled under these conditions, yielding a predicted ~8-fold increase of the detectable signal relative to tightly focused laser conditions.

This approach was employed to analyze a model system of a 400 mesh London finder grid coated with vapor-deposited β-estradiol and attached to indium foil. By varying the position of the focusing lens in the direction of beam propagation ("z-scan"), the focal diameter was varied until the molecular ion signal was maximized. This condition was found for a focal diameter of ~350 μm, corresponding to an optimized intensity $I_0 \approx 4 \times 10^{13}$ W/cm^2, which corroborates the optimization strategy outlined above. The observed 10-fold increase in signal between the focused and optimized laser beam is in good agreement with the prediction derived from the indium data, indicating that the shape of the detectable plume does not undergo drastic changes between atoms and molecules desorbed by C_{60} impact.

A comparison of the gas phase, SFI-SNMS, and SIMS spectra obtained under these conditions is shown in Figure 7. The SIMS signal was obtained without the postionization laser and the secondary ion suppression pulse, but under otherwise identical experimental conditions. It is obvious that the relative amount of fragmentation observed in the SFI-SNMS spectrum far exceeds that in the other spectra. As outlined above, this is partially the result of the intact ionization of sputtered neutral fragments but can also be due to the photodissociation of intact molecules sputtered with sufficient internal energies to alter their ionization mechanism. However, despite the increased fragmentation and incomplete overlap with the sputtered

dx.doi.org/10.1021/jp5080708 | J. Phys. Chem. C 2014, 118, 25534–25544

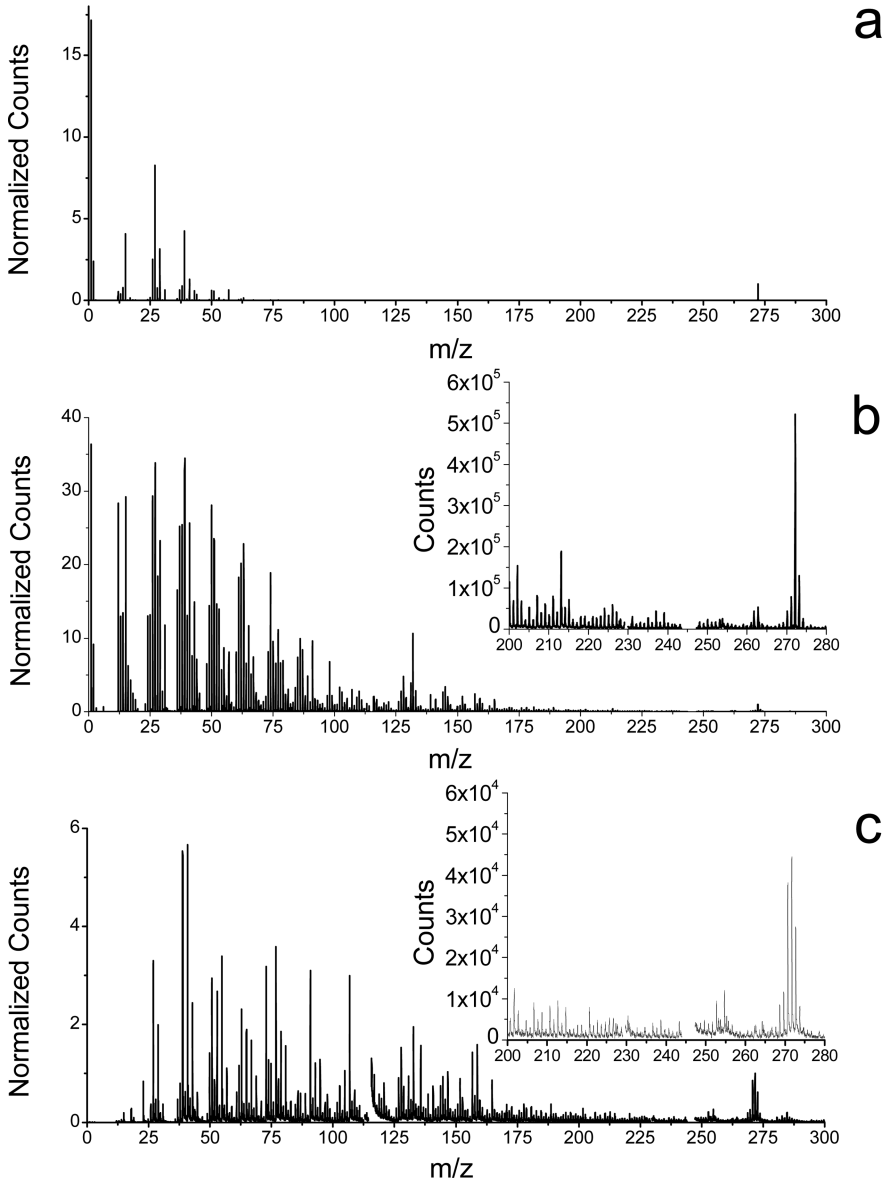

Figure 7. Comparison of gas phase, SNMS, and SIMS spectra of β-estradiol. The spectra are normalized to their respective molecular ion signal, while the insets are experimental counts. (a) Gas phase ionization with $I \approx 5 \times 10^{13}$ W/cm^2 at 1350 nm. (b) Optimized SFI SNMS analysis with a defocused laser beam at $I \approx 4 \times 10^{13}$ W/cm^2 at 1350 nm. (c) SIMS spectra from a London finder grid vapor deposited with β-estradiol and attached to indium foil (discontinuity in the mass spectra are subtracted In monomer, dimer, and oxide signals).

plume, the postionized molecular ion signal of β-estradiol is over an order of magnitude higher than the secondary ion signal in SIMS. Given the estimated plume overlap as determined above, one could expect a further increase of about a factor 4 under conditions where the entire detectable plume of sputtered neutral particles could be sampled.

This increase in sensitivity for a biologically relevant molecule is indeed significant. We believe that it opens the possibility to extend the capabilities of SIMS in bioimaging applications where limited concentrations of analyte, small analysis areas, and/or matrix effects limit the secondary ion signal. An example of the improvement in image quality enabled by this SNMS approach over SIMS is presented in Figure 8. The greater SFI neutral signal markedly improves the visible resolution and imaging quality of this model system.

The obtained images can be used to determine the geometric variation of the plume overlap as a function of the ion beam position. If the ion beam is directed to different pixels of the image, the sputtered particles emerge from a point source

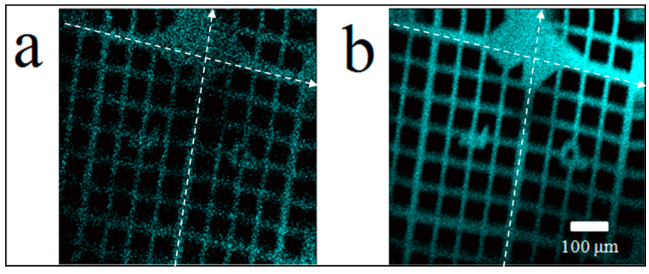

Figure 8. (a) SIMS (total M^+ counts 1.92×10^7) and (b) SNMS (total M^+ counts 2.26×10^8) images of the molecular ion of β-estradiol, with the sterol vapor deposited onto a 400 mesh Ni London finder grid. Postionization was performed at 1350 nm with an intensity of $I \approx 4 \times 10^{13}$ W/cm^2. Dashed arrows represent line scans discussed in the text.

dx.doi.org/10.1021/jp5080708 | J. Phys. Chem. C 2014, 118, 25534−25544

located at different lateral positions with respect to the laser beam. The neutral particles intercepted by the laser must therefore be emitted under different angles and may exhibit a different probability of being transmitted through the mass spectrometer after ionization. The magnitude of this effect is hard to calculate, since it requires detailed knowledge about the emission angle and velocity distribution of the sputtered particles. It can, however, be quantitatively estimated from the comparison of the two images displayed in Figure 8. Secondary ions emerge from the surface already in a charged state and form a plume, which is sampled by the TOF spectrometer upon switching the extraction field. The variation of the secondary ion signal across the line scans as indicated in Figure 8 therefore reveals the geometry dependent change of the detectable sputtered plume. Neutral particles can be assumed to form a similar plume of particles that are in principle detectable by the mass spectrometer, but must in addition be intercepted and postionized by the laser. The ratio of corresponding line scans along the same lines in Figure 8a,b therefore allows a direct determination of the plume overlap factor as a function of the ion beam position at the surface. The results obtained for the two indicated lines are depicted in Figure 9. In order to

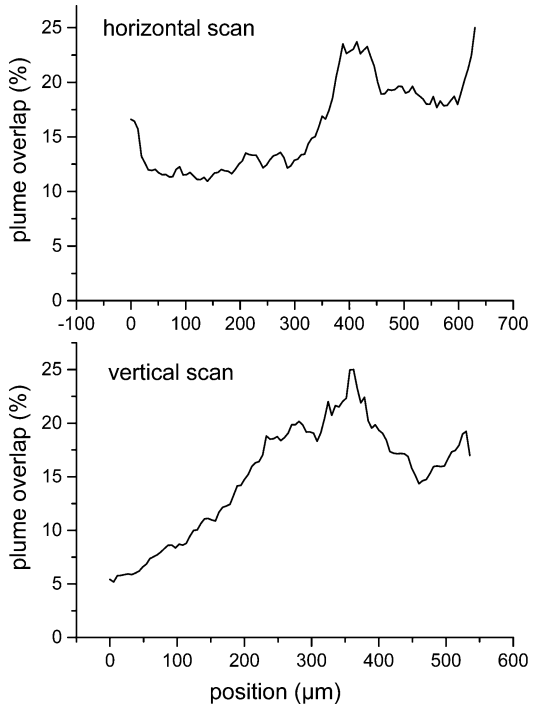

Figure 9. Variation of geometric overlap between detectable plume of sputtered particles and postionization laser as determined from the ratio of line scans across the two images of Figure 8. The *y*-axis was scaled to the maximum plume overlap discussed in the text.

interpret the data, it is of note that the laser beam propagates in an approximately diagonal direction from the lower left to the upper right corner of the image, so that both scan lines form about the same angle with the beam direction. It is apparent that the best overlap is achieved if the surface is bombarded at a spot that is slightly displaced from the center toward the upper right corner of the image. Although the overlap is found to decrease with increasing distance from that optimum location, the overall variation across the image is mostly within a factor 2, demonstrating that practical imaging experiments at extended field of view can be done with the current system. In order to achieve an even more uniform overlap over larger fields of view, one could in principle imagine scanning the laser beam synchronously with the primary ion beam.

CONCLUSION

The present experiments demonstrate that strong field ionization is a useful tool to extend the application of ion beam induced mass spectrometry techniques for molecular imaging. As a case study, we investigated β-estradiol, a hormone whose structure is similar to a class of biologically important sterols. Combining a fundamental study of the ionization behavior of this molecule with respect to wavelength and intensity of the ionizing laser with strategies to enhance its practical application, we show that the molecular ion signal in a model SNMS β-estradiol imaging experiment can be increased to over an order of magnitude higher than the corresponding SIMS signal. On the basis of future developments in laser technology, one can expect to increase this enhancement even further once more powerful laser systems become available. The present laser system achieves 25% overlap with the sputtered plume, and since our observed enhancement factor for the molecular ion is ~10, we expect that a 40-fold increase may be possible with a higher power system. This value is exciting, since it delivers the first experimental evidence for a long-discussed topic related to the ionization probability (or, more accurately, the ion fraction) of sputtered organic molecules. From the data obtained here, it is evident that the probability of an intact β-estradiol molecule to be desorbed from the surface as a positive secondary ion cannot be larger than about 2.5%. In fact, the ion fraction is likely to be even lower due to the unknown photofragmentation probability accompanying the laser postionization process, thus imposing a severe limit to the observable molecular secondary ion yield. The observed level of improvement that can be expected from strong field laser postionization provides a compelling reason for the future adoption of strong field laser postionization in bioanalysis applications where SIMS is challenged by low analyte concentrations and matrix effects. The results reported here are remarkable since the sterol molecule is not extensively conjugated and contains σ bonds, which are known to be prone to fragmentation upon laser postionization. It therefore seems likely that these protocols should be applicable to a wide range of other molecules as well.

ASSOCIATED CONTENT

Supporting Information

Description of the theoretical model underlying the definition of the saturation intensity along with Figure S-1 showing additional data on strong field ionization studies of gas phase Xe atoms and its interpretation in order to calibrate the laser intensity. This material is available free of charge via the Internet at http://pubs.acs.org.

AUTHOR INFORMATION

Corresponding Author

*E-mail: nxw@psu.edu (N.W.).

Notes

The authors declare no competing financial interest.

■ ACKNOWLEDGMENTS

Financial support from the U.S. Department of Energy, Division of Chemical Sciences, Basic Energy Sciences, under grant DE-FG02-06ER15803 is gratefully acknowledged. Dr. David Willingham's design and construction of the vapor deposition chamber used in these experiments is acknowledged and appreciated.

■ ADDITIONAL NOTES

[a]Signals below m/z 40 were detected with intensities that saturated the transient digitizer used to register the TOF spectrum and could therefore not be interpreted in a quantitative manner.

[b]Note that the sputtered molecule may in principle contain more internal energy which is not available to reduce the effective ionization threshold.[49]

[c]Note that the spot diameter refers to the standard optical definition (2 times the radius where the intensity drops to I_0/e^2), while R is the radius defined by I_0/e.

■ REFERENCES

(1) Ninomiya, S.; Nakata, Y.; Ichiki, K.; Seki, T.; Aoki, T.; Matsuo, J. Measurements of Secondary Ions Emitted from Organic Compounds Bombarded with Large Gas Cluster Ions. *Nucl. Instrum. Methods Phys. Res., Sect. B* **2007**, *256*, 493−496.

(2) Rabbani, S.; Barber, A. M.; Fletcher, J. S.; Lockyer, N. P.; Vickerman, J. C. Tof-Sims with Argon Gas Cluster Ion Beams: A Comparison with C-60(+). *Anal. Chem.* **2011**, *83*, 3793−3800.

(3) Smith, D. F.; Robinson, E. W.; Tolmachev, A. V.; Heeren, R. M. A.; Pasa-Tolic, L. C-60 Secondary Ion Fourier Transform Ion Cyclotron Resonance Mass Spectrometry. *Anal. Chem.* **2011**, *83*, 9552−9556.

(4) Fletcher, J. S.; Vickerman, J. C.; Winograd, N. Label Free Biochemical 2d and 3d Imaging Using Secondary Ion Mass Spectrometry. *Curr. Opin. Chem. Biol.* **2011**, *15*, 733−740.

(5) Fletcher, J. S.; Vickerman, J. C. Secondary Ion Mass Spectrometry: Characterizing Complex Samples in Two and Three Dimensions. *Anal. Chem.* **2013**, *85*, 610−639.

(6) Winograd, N.; Baxter, J. P.; Kimock, F. M. Multi-Photon Resonance Ionization of Sputtered Neutrals - a Novel-Approach to Materials Characterization. *Chem. Phys. Lett.* **1982**, *88*, 581−584.

(7) Becker, C. H.; Gillen, K. T. Surface-Analysis by Nonresonant Multiphoton Ionization of Desorbed or Sputtered Species. *Anal. Chem.* **1984**, *56*, 1671−1674.

(8) Dyer, M. J.; Jusinski, L. E.; Helm, H.; Becker, C. H. Surface-Analysis by Photoionization of Sputtered Species with Intense Picosecond Laser-Radiation. *Appl. Surf. Sci.* **1991**, *52*, 151−157.

(9) Terhorst, M.; M?llers, R.; Niehuis, E.; Benninghoven, A. High-Spatial-Resolution Surface Imaging of Inorganic and Organic Structures by Multiphoton Post-Ionization of Sputtered Neutrals and Time-of-Flight Mass-Spectrometry. *Surf. Interface Anal.* **1992**, *18*, 824−826.

(10) Winograd, N. Ion-Beams and Laser Postionization for Molecule-Specific Imaging. *Anal. Chem.* **1993**, *65*, A622−A629.

(11) Brummel, C. L.; Willey, K. F.; Vickerman, J. C.; Winograd, N. Ion-Beam-Induced Desorption with Postionization Using High Repetition Femtosecond Lasers. *Int. J. Mass Spectrom. Ion Processes* **1995**, *143*, 257−270.

(12) Willingham, D.; Kucher, A.; Winograd, N. Strong-Field Ionization of Sputtered Molecules for Biomolecular Imaging. *Chem. Phys. Lett.* **2009**, *468*, 264−269.

(13) Veryovkin, I. V.; Calaway, W. F.; Tripa, C. E.; Moore, J. F.; Wucher, A.; Pellin, M. J. Laser Post-Ionization Secondary Neutral Mass Spectrometry for Ultra-Trace Analysis of Samples from Space Return Missions. *Nucl. Instrum. Methods Phys. Res., Sect. B* **2005**, *241*, 356−360.

(14) Veryovkin, I. V.; Calaway, W. F.; Tripa, C. E.; Pellin, M. J. Mass Spectrometry on the Nanoscale with Ion Sputtering Based Techniques: What Is Feasible. *Nucl. Instrum. Methods Phys. Res., Sect. B* **2007**, *261*, 508−511.

(15) Schuhle, U.; Pallix, J. B.; Becker, C. H. Sensitive Mass-Spectrometry of Molecular Adsorbates by Stimulated Desorption and Single-Photon Ionization. *J. Am. Chem. Soc.* **1988**, *110*, 2323−2324.

(16) Tyler, B. J.; Dambach, S.; Galla, S.; Peterson, R. E.; Arlinghaus, H. F. Investigation of the Utility of Laser-Secondary Neutral Mass Spectrometry for the Detection of Polyaromatic Hydrocarbons in Individual Atmospheric Aerosol Particles. *Anal. Chem.* **2012**, *84*, 76−82.

(17) Hrubowchak, D. M.; Ervin, M. H.; Wood, M. C.; Winograd, N. Detection of Biomolecules on Surfaces Using Ion-Beam-Induced Desorption and Multiphoton Resonance Ionization. *Anal. Chem.* **1991**, *63*, 1947−1953.

(18) Willey, K. F.; Brummel, C. L.; Winograd, N. Photoionization Mechanisms for Cr(Co)(6) Using High Intensity Laser Pulses in the near-IR. *Chem. Phys. Lett.* **1997**, *267*, 359−364.

(19) Willey, K. F.; Vorsa, V.; Braun, R. M.; Winograd, N. Postionization of Molecules Desorbed from Surfaces by Kev Ion Bombardment with Femtosecond Laser Pulses. *Rapid Commun. Mass Spectrom.* **1998**, *12*, 1253−1260.

(20) Vorsa, V.; Kono, T.; Willey, K. F.; Winograd, N. Femtosecond Photoionization of Ion Beam Desorbed Aliphatic and Aromatic Amino Acids: Fragmentation Via Alpha-Cleavage Reactions. *J. Phys. Chem. B* **1999**, *103*, 7889−7895.

(21) Vorsa, V.; Willey, K. F.; Winograd, N. Photoionization of Gas-Phase Versus Ion-Beam-Desorbed Dopamine with Femtosecond Laser Pulses. *Anal. Chem.* **1999**, *71*, 574−581.

(22) Boguslavskiy, A. E.; Mikosch, J.; Gijsbertsen, A.; Spanner, M.; Patchkovskii, S.; Gador, N.; Vrakking, M. J. J.; Stolow, A. The Multielectron Ionization Dynamics Underlying Attosecond Strong-Field Spectroscopies. *Science* **2012**, *335*, 1336−1340.

(23) Krausz, F.; Ivanov, M. Attosecond Physics. *Rev. Mod. Phys.* **2009**, *81*, 163−234.

(24) Levis, R. J.; DeWitt, M. J. Photoexcitation, Ionization, and Dissociation of Molecules Using Intense Near-Infrared Radiation of Femtosecond Duration. *J. Phys. Chem. A* **1999**, *103*, 6493−6507.

(25) Lezius, M.; Blanchet, V.; Rayner, D. M.; Villeneuve, D. M.; Stolow, A.; Ivanov, M. Y. Nonadiabatic Multielectron Dynamics in Strong Field Molecular Ionization. *Phys. Rev. Lett.* **2001**, *86*, 51−54.

(26) Lezius, M.; Blanchet, V.; Ivanov, M. Y.; Stolow, A. Polyatomic Molecules in Strong Laser Fields: Nonadiabatic Multielectron Dynamics. *J. Chem. Phys.* **2002**, *117*, 1575−1588.

(27) Markevitch, A. N.; Smith, S. M.; Romanov, D. A.; Schlegel, H. B.; Ivanov, M. Y.; Levis, R. J. Nonadiabatic Dynamics of Polyatomic Molecules and Ions in Strong Laser Fields. *Phys. Rev. A* **2003**, *68*, 011402.

(28) Markevitch, A. N.; Romanov, D. A.; Smith, S. M.; Schlegel, H. B.; Ivanov, M. Y.; Levis, R. J. Sequential Nonadiabatic Excitation of Large Molecules and Ions Driven by Strong Laser Fields. *Phys. Rev. A* **2004**, *69*, 013401.

(29) Smith, S. M.; Li, X. S.; Markevitch, A. N.; Romanov, D. A.; Levis, R. J.; Schlegel, H. B. Numerical Simulation of Nonadiabatic Electron Excitation in the Strong Field Regime. 2. Linear Polyene Cations. *J. Phys. Chem. A* **2005**, *109*, 10527−10534.

(30) Smith, S. M.; Li, X. S.; Markevitch, A. N.; Romanov, D. A.; Levis, R. J.; Schlegel, H. B. A Numerical Simulation of Nonadiabatic Electron Excitation in the Strong Field Regime: Linear Polyenes. *J. Phys. Chem. A* **2005**, *109*, 5176−5185.

(31) Markevitch, A. N.; Romanov, D. A.; Smith, S. M.; Levis, R. J. Rapid Proton Transfer Mediated by a Strong Laser Field, *Phys. Rev. Lett.* **2006**, *96*.

(32) Markevitch, A. N.; Romanov, D. A.; Smith, S. M.; Levis, R. J. Probing Strong-Field Electron-Nuclear Dynamics of Polyatomic Molecules Using Proton Motion, *Phys. Rev. A* **2007**, *75*.

(33) Smith, S. M.; Li, X. S.; Markevitch, A.; Romanov, D.; Levis, R. J.; Schlegel, H. B. Numerical Simulation of Nonadiabatic Electron

Excitation in the Strong-Field Regime. 3. Polyacene Neutrals and Cations. *J. Phys. Chem. A* **2007**, *111*, 6920−6932.
(34) Smith, S. M.; Romanov, D. A.; Heck, G.; Schlegel, H. B.; Levis, R. J. Observing the Transition from Stark-Shifted, Strong-Field Resonance to Nonadiabatic Excitation. *J. Phys. Chem. C* **2010**, *114*, 5645−5651.
(35) Smith, S. M.; Romanov, D. A.; Li, X. S.; Sonk, J. A.; Schlegel, H. B.; Levis, R. J. Numerical Bound State Electron Dynamics of Carbon Dioxide in the Strong-Field Regime. *J. Phys. Chem. A* **2010**, *114*, 2576−2587.
(36) Kotur, M.; Weinacht, T. C.; Zhou, C. Y.; Matsika, S. Strong-Field Molecular Ionization from Multiple Orbitals. *Phys. Rev. X* **2011**, *1*, 021010.
(37) Spanner, M.; Patchkovskii, S.; Zhou, C. Y.; Matsika, S.; Kotur, M.; Weinacht, T. C. Dyson Norms in Xuv and Strong-Field Ionization of Polyatomics: Cytosine and Uracil. *Phys. Rev. A* **2012**, *86*, 050301.
(38) Ammosov, M. V.; Delone, N. B.; Krainov, V. B. Tunnel Ionization of Complex Atoms and Atomic Ions in Alternating Electromagnetic Fields. *Sov. Phys.—JETP* **1986**, *64*, 1191−1194.
(39) Hankin, S. M.; Villeneuve, D. M.; Corkum, P. B.; Rayner, D. M. Intense-Field Laser Ionization Rates in Atoms and Molecules. *Phys. Rev. A* **2001**, *64*, 013405−013412.
(40) Trebino, R.; Bowlan, P.; Gabolde, P.; Gu, X.; Akturk, S.; Kimmel, M. Simple Devices for Measuring Complex Ultrashort Pulses. *Laser Photon. Rev.* **2009**, *3*, 314−342.
(41) Gingras, G.; Tripathi, A.; Witzel, B. Wavelength and Intensity Dependence of Short Pulse Laser Xenon Double Ionization between 500 and 2300 nm. *Phys. Rev. Lett.* **2009**, *103*, 173001.
(42) Braun, R. M.; Blenkinsopp, P.; Mullock, S. J.; Corlett, C.; Willey, K. F.; Vickerman, J. C.; Winograd, N. Performance Characteristics of a Chemical Imaging Time-of-Flight Mass Spectrometer. *Rapid Commun. Mass Spectrom.* **1998**, *12*, 1246−1252.
(43) Weibel, D.; Wong, S.; Lockyer, N.; Blenkinsopp, P.; Hill, R.; Vickerman, J. C. A C-60 Primary Ion Beam System for Time of Flight Secondary Ion Mass Spectrometry: Its Development and Secondary Ion Yield Characteristics. *Anal. Chem.* **2003**, *75*, 1754−1764.
(44) Wucher, A. Laser Postionization - Fundamentals. In *TOF-SIMS: Materials Analysis by Mass Spectrometry*, 2nd ed.; Vickerman, J. C., Briggs, D., Eds.; IM Publications and Surface Spectra: Chichester, UK, 2013; pp 217−246.
(45) Fraser, G. W. The Gain, Temporal Resolution and Magnetic-Field Immunity of Microchannel Plates. *Nucl. Instrum. Methods Phys. Res., Sect. A* **1990**, *291*, 595−606.
(46) Takahata, Y.; Vendrame, R. Ionization Energies, Electron Affinities and Excitation Energies of Some Steroid Hormones Calculated with the Semiempirical Ham/3 Method. *J. Braz. Chem. Soc.* **2001**, *12*, 165−172.
(47) Wucher, A. Internal Energy of Sputtered Metal Clusters. *Phys. Rev. B* **1994**, *49*, 2012−2020.
(48) Takahashi, L. K.; Zhou, J.; Wilson, K. R.; Leone, S. R.; Ahmed, M. Imaging with Mass Spectrometry: A Secondary Ion and VUV-Photoionization Study of Ion-Sputtered Atoms and Clusters from GaAs and Au. *J. Phys. Chem. A* **2009**, *113*, 4035−4044.
(49) Wucher, A.; Staudt, C.; Neukermans, S.; Janssens, E.; Vanhoutte, F.; Silverans, R. E.; Lievens, P. On the Internal Energy of Sputtered Clusters. *New J. Phys.* **2008**, *10*, 1−22.
(50) Garrison, B. J.; Postawa, Z.; Ryan, K. E.; Vickerman, J. C.; Webb, R. P.; Winograd, N. Internal Energy of Molecules Ejected Due to Energetic C_{60} Bombardment. *Anal. Chem.* **2009**, *81*, 2260−2267.
(51) Brenes, D. A.; Garrison, B. J.; Winograd, N.; Postawa, Z.; Wucher, A.; Blenkinsopp, P. Fluid Flow and Effusive Desorption: Dominant Mechanisms of Energy Dissipation after Energetic Cluster Bombardment of Molecular Solids. *J. Phys. Chem. Lett.* **2011**, *2*, 2009−2014.
(52) Breuer, L.; Kucher, A.; Herder, M.; Wucher, A.; Winograd, N. Formation of Neutral Inncm Clusters under C_{60} Ion Bombardment of Indium. *J. Phys. Chem. A* **2014**, *118*, 85542−8552.